Energy Conversion and Management, Volume 237, June 2021, Article number 114107
DOI:10.1016/j.enconman.2021.114107

Techno-Economic Evaluation and Optimization of CCGT Power Plant: A Multi-Criteria Decision Support System

Yu-Zhi Chen[a,b], Yi-Guang Li[b,*], Elias Tsoutsanis[c], Mike Newby[d], and Xu-Dong Zhao[a]

[*] Corresponding author (i.y.li@cranfield.ac.uk)

[a] *Key Laboratory of Intelligent Control and Optimization for Industrial Equipment, Dalian University of Technology, P.R. China*

[b] *School of Aerospace, Transport and Manufacturing, Cranfield University, Bedford, MK43 0AL, UK*

[c] *Department of Mechanical Engineering, University of Birmingham, Edgbaston, Birmingham, B15 2TT, UK*

[d] *Manx Utilities, Douglas, Isle of Man, UK*

ABSTRACT

A key objective of the power generation industry is to achieve maximum economic benefit without over-consuming the life of power plants and over-maintaining its assets. From a CCGT power plant operator's perspective, the stand-alone performance of the plant is not enough to support the decision-making process due to the plethora of possible scenarios characterized by variable ambient conditions, engine health (fouling, erosion), electricity prices, and power demand. This study proposes a novel methodology to support decision-making for a CCGT power plant's operational optimization. The comprehensive techno-economic performance evaluation is conducted by multidisciplinary optimization and decision-making to enhance information integration for the combined cycle power plant operated by Manx Utilities in the Isle of Man, UK. The decision support system has the capability to recommend the optimal operation schedules to plant operators. It recommends that the more severely degraded engine should run at a relatively lower power setting to decrease creep life consumption. The established power plant optimization framework has the potential to assist power plant operators in deciding the total power output and power split between gas turbines based on optimization results that considers both immediate thermo-economic benefits and life consumption. Finally, the proposed system can facilitate similar power plants to adjust daily operations to achieve thermo-economic and lifing benefits.

Key Words: Thermo-economics, Thermodynamics, Combined cycle gas turbine, Creep life, Emission, Multi-criteria optimization, Decision-making

Nomenclature

cd	=	Cumulative distance
C	=	Constant
CD	=	Dimensionless cumulative distance
CF	=	Creep factor
C_aH_b	=	Hydrocarbon fuel
CS	=	Closeness to the ideal design
d	=	Distance between adjacent points
EC	=	Emission cost (£/s)
ESP	=	Electricity selling price (£/kWh)
FC	=	Fuel cost (£/s)
FF	=	Fuel flow rate (kg/s)
FP	=	Fuel price (pence/therm)
$Income$	=	Income from selling electricity
LF	=	Life fraction
LHV	=	Low heating value (J/kg)
LMP	=	Laron-Miller Parameter
MSC	=	Maintenance and staff cost (£/s)
OT	=	Operating time (hours)
PO	=	Power output (MW)
S^-	=	Pareto Front to the ideal worst position
S^+	=	Pareto Front to the ideal best position
SS	=	Spark spread (£)
t_f	=	Time to failure (hours)
t_{ref}	=	Reference time to failure (hours)
T_m	=	Metal temperature (Kelvin)

Tax_{CO_2} = Carbon dioxides taxes (£/s)

w = Weight factor

W = Normalized weight factor

W_{CO_2} = Mass flow rate of carbon dioxide (kg/s)

y_{ij} = The jth criteria for ith Pareto Front

z_{ij} = The normalized jth criteria for ith Pareto Front

Subscripts

a = Number of involved carbon molecules

b = Number of involved hydrogen molecules

cable = Interconnecting electricity cable

Eq = Equivalent

GT = Gas turbine

island = Local island

Ref = Reference value for data dimensionless

total = Sum of local island and grid

1. Introduction

Global net electricity generation is expected to rise by more than 80% between 2018 and 2050 [1]. Since fossil-fuel occupies more than 65% of the energy for electricity generation worldwide [2], decreasing fossil fuel reserves together with the ecological impact of fossil-fuel power plants has recently attracted the attention of the public [3,4]. Many suggestions have been made for mitigating the environmental impact, meeting sustainable energy targets and optimizing power plants to make them more energy-efficient while continuing to have a role supporting renewables [3,5,6].

One of the most significant concerns of plant stakeholders is the maintenance cost. For example, 51.34 million Euros is predicted as the maintenance cost of a SIEMENS V94.3A gas turbine (GT), which is 17.9 times more than the capital cost of 2.86 million Euros [7]. Consequently, a growing body of literature has emphasised the importance

of running a power plant with advanced efficiency, high economic benefit, low emissions, and extended time between failures to reduce maintenance costs. The majority of the research has focused on design considerations and the selection of power generating equipment. The selection criteria have included the number of heat engines, the heat engines' configuration, working fluid, and individual engine/equipment capacity.

Baccioli et al. (2017) [8] presented a novel configuration of an organic flash cycle for recovering the waste heat at low temperatures and eight kinds of organic fluids were tested to find the optimum medium. Brighenti et al. (2017) [9] proposed a single objective optimization system for a humid air turbine power plant to maximize the plant's thermal efficiency at the design point. Ondeck et al. (2017) [10] analyzed the combined heat and power (CHP) equipment structure optimization working in island mode using temporal Lagrangean decomposition. Palagi et al. (2019) [11] reported a plant design platform to optimize the thermodynamic performance of an organic Rankine cycle (ORC). Frate et al. (2019) [12] after a thorough techno-economic review of a power plant recommended replacing the throttling valve with a steam expander. Yang et al. (2020) [13] analyzed multi-objective optimization for designing combined cooling, heating, and power systems with a supercritical carbon dioxide recompression Brayton cycle to maximize the electricity efficiency and total product.

Mohammadi et al. (2020) [14] conducted a systematic study to design a new triple cycle plant by optimizing the levelized cost of electricity. Liu and He (2020) [15] studied parametric optimization of an ORC during the design stage to integrate with a GT-modular helium reactor. Su et al. (2020) [16] introduced a multi-objective optimization platform for a combined GT /supercritical CO_2 (S-CO_2) recompression / transcritical CO2 cogeneration system to optimize the thermodynamic performance and investment cost simultaneously. Chen et al. (2020) [17] conducted a power and efficiency optimization through a parametric study of the design an advanced Maisotsenko-Brayton cycle. Sayyaadi et al. (2020) [17] reported an optimizing multi-objective survey to find the optimum secondary bottoming cycle among different technologies when recovering low-grade thermal energy from a GT. Movahed and Avami (2020) [18] optimized the design of a combined cooling, heating, and power generation system for a wastewater treatment plant by considering the total cost rate and production of biogas as two objective functions.

Pan et al. (2020) [19] conducted a multi-objective optimization analysis for a dual turbine-alternator-compressor S-CO2 recompression Brayton cycle, by considering thermo-economic aspects at the design stage. Zare (2020) [20] investigated the design concept of inlet cooling through the absorption refrigeration cycle for a GT when considering levelized cost and efficiency as two optimization objectives. Song et al. (2020) [21] introduced an optimization

platform for a combined cooling, heating, and power system to optimize both economic and energy-saving performances. Badshah et al. (2020) [22] reported an optimized high-temperature heat exchanger design in an externally fired GT. Jalili et al. (2021) [6] conducted ecological and economic analyses based on emergy to optimize the energy investment of power generation systems.

A growing body of literature is focusing on the theme of power generating operation optimization [23]. Walsh and Fletcher (2004) [24] provided an example based on the net present value assessment when establishing a new combined-cycle gas turbine (CCGT) power plant. Wang et al. (2020) [25] introduced an operation optimization scheme for a steam generator that can reduce the molten salt consumption by 0.98-13.68% compared to the original system. Milosavljevic et al. (2020) [26] suggested load-sharing optimization for gas compressors, in which power consumption gives up to 10% less yield than the original equal load distribution. Kim et al. (2020) developed an optimization system for CHP based on a neural network where the computation speed of their method is more than 7000 times faster than the physics-based model.

Faridpak et al. (2020) [27] proposed a series of multi-step schemes to minimize the cost of an integrated power and gas system, in which surrogate Lagrangian relaxation is applied to accelerate the optimization process. Zhou et al. (2020) [28] performed a tiered gas tariff model to optimize the cost of energy between residential and other regions, potentially decreasing the overall operation cost of multi-region gas and power complementary systems. Chen et al. (2020) [29] conducted an economy and risk study of an integrated natural gas and heating water transmission system, which considered the dynamic characteristics and uncertainty during optimal operation. Zhang et al. (2020) [3] investigated distributional optimization for an electricity-gas coupled system through a data-driven method to minimize operating costs. Yazdi et al. (2020) [30] studied three different kinds of inlet air cooling systems to optimize gas turbine operation characteristics, such as fuel consumption, cost of electricity production, or pollutants.

The majority of the reported literature deals with thermo-economic aspects and thermal equipment under clean/nominal conditions. However, thermal equipment life consumption is a significant concern of plant stakeholders as it is directly related to the forced outage downtime as well as negatively impacting on thermal equipment degradation and a range of other operating, environmental, and lifing issues.

Typically, in many classic studies, maintenance cost is considered to represent the GT's life usage through economic cost, which is related to the power output only through a constant annual fee [10,31] or capital cost [13,15,19,21]. However, maintenance costs are deeply affected by the GT hot section life consumption, where engine

health state degradation is more prominent and non-recoverable and this has not been considered in the maintenance cost models [10,13,15,19,21,31,32]. In previously published studies [26,33–35], the plant's total power setting was deemed to be constant for each condition, and thermodynamic/thermo-economic optimization was applied to determine the power distribution between different engine sets.

Plant operation optimization under different health conditions among parallel units has received insufficient attention, and an optimized plant power setting through a life consumption perspective raises an interesting concern. To the authors' best knowledge, this is the first study in the open literature where the topping cycle hot section life usage is considered in load sharing and integrated into the economic aspects for a multi-criteria optimization of a CCGT power plant. The present research explores how topping cycle health and hot section lifing may be considered during plant operation optimization.

To address the gaps, mentioned above, in the open literature, a decision support framework is proposed to optimize the power plant's daily operation to decide the total power output and power split between different engine sets where both thermo-economics and GT hot section lifing are simultaneously optimized by a multi-criteria genetic algorithm (MCGA). The decision support framework is designed to optimize the CCGT power plant's daily generation schedule. The Technique for Order Preference by Similarity to Ideal Solution (TOPSIS) [13] is adapted in this study for multi-criteria decision-making from the Pareto Front obtained by the genetic algorithm. To this end, the contributions of this study are summarized as follows:

1) A novel decision support framework is developed for thermo-economic and lifing optimization of a CCGT power plant for daily operation. This framework moves the operation from an equal load power split to a load-sharing optimization-based operation to improve the thermo-economic and life consumption performances.
2) Adapted TOPSIS is proposed as a multi-criteria decision-making tool to select the power plant's optimal operation scheme based on the Pareto Front obtained by a MCGA.
3) Experimental results from a CCGT power plant representative of a typical day's operation have been used to decide the total power output and power split between the two GTs that form the system for varying power demand, GT engine health states, ambient conditions, and electricity price.
4) The novel optimization scheme should decrease the GT hot section's life consumption without loss of thermo-economic performance when the two GTs are in different health states.

The remainder of the paper is organized as follows. The second section is concerned with the system model used for this study and introduces the optimization algorithm and the decision-making method. Section 3 highlights the proposed multi-criteria decision support system for techno-economic performance evaluation and optimization of the CCGT being considered. The fourth section presents the findings of the case study for the CCGT power plant. The last section presents the conclusions of this study.

2. System Modelling

2.1 System Configuration and Description

As a statutory board of the local authorities, Manx Utilities (MU) has the responsibility to provide a reliable and efficient electricity supply to the Isle of Man in the United Kingdom. Pulrose Power Station, of concern here, belongs to MU. This is a CCGT power plant that includes two General Electric LM2500+ dual-shaft aero-derivative GTs (i.e., GT6 & GT7) [36], two Innovative Steam Technologies C01049 parallel dual-pressure once-through steam generators (i.e., OTSG6, OTSG7) [37] and a MAN Turbo DK080/250RZ1 steam turbine (i.e., ST8) [36]. The power plant's design point specification can be found in Table 1 [36], and the schematic of the power plant is shown in Fig. 1. MU also owns a 45 MVA subsea electricity cable connected to the North West of England's distribution system. Both imports and exports of electricity can be achieved via the cable, in which electricity services are traded between MU and the UK electricity network.

The following assumptions are applied to simplify the models without compromising the accuracy of the system modeling:

1) The power plant is operating under steady-state conditions.
2) The low cycle fatigue life consumption is not considered in this study due to the fact that the gas turbines involved in this study experience less frequent start-ups and shutdowns and the creep damage dominates the life consumption of the engines.
3) The power required by auxiliary systems (feed water pumps, cooling water circulation pumps, etc.) is constant under off-design conditions.
4) The cooling cycle for the condenser is ignored.
5) The loss of power during transmission via the electricity cable is ignored, and the cable's electricity purchase price is assumed the same as the selling price to the island residents.

6) The calculation of carbon dioxide (CO_2) emission is based on chemical equilibrium.

7) The power plant has two GTs driving a steam cycle with two OTSGs and one steam turbine.

8) As the power plant is rarely operated at less than 23 MW for steady-state conditions, each GT's minimum power is assumed to be 23 MW. The GT shuts down if the power demand on the GT is below 23 MW.

9) The profile data for ambient temperature, island power demand, maximum allowed power generation, electricity trading prices, fuel gas prices, etc., are available and based on the power plant tracking the team's prediction results in advance while the prediction uncertainty is ignored.

10) The steam cycle is always in operation to ensure high power plant efficiency.

Table 1 CCGT specifications [36]**.**

Symbol	Parameter	Value	Units
PO_{GT}	GT Power Output	32	MW
HR	Heat Rate	9734	kJ/kWh
PR	GT Pressure Ratio	23.1	-
N_{GG}	GT Gas Generator Speed	9000	rpm
N_{PT}	GT Power Turbine Speed	6100	rpm
T_{exh}	GT Exhaust Gas Temperature	498	℃
W_{exh}	GT Exhaust Gas Mass Flow Rate	89.09	kg/s
P_{HP}	High-pressure (HP) Steam Pressure	56.81	bar
T_{HP}	HP Steam Temperature	484	℃
W_{HP}	HP Steam Mass Flow Rate	9.58	kg/s
P_{LP}	Low-pressure (LP) Steam Pressure	6.89	bar
T_{LP}	LP Steam Temperature	258	℃
W_{LP}	LP Steam Mass Flow Rate	2.25	kg/s
T_{stk}	OTSG Stack Temperature	120	℃
PO_{ST}	ST Power Output	23	MW
N_{ST}	ST Turbine Speed	4818	rpm
x	ST Exhaust Steam Wetness	11.7	%
P_{cond}	ST Exhaust Steam Pressure	0.06	bar

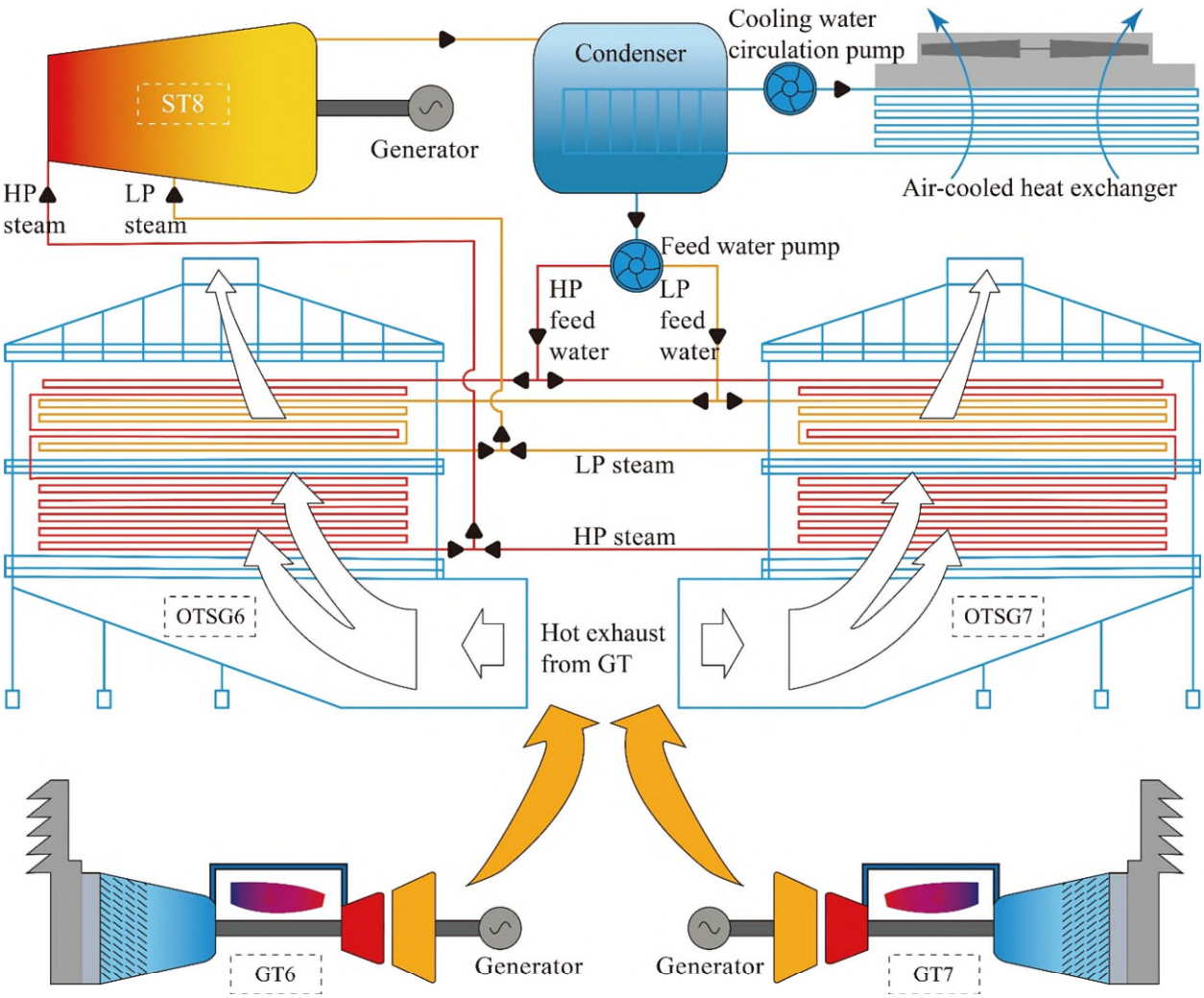

Fig. 1 Schematic layout of Manx Utilities CCGT power plant.

2.2 Mathematical Model of Combined-Cycle Gas Turbine

The CCGT performance, including the GT, OTSG, and ST thermodynamic models is introduced first. The thermodynamic models previously developed by the authors and published in [38–47] are used in this study.

2.2.1 Gas Turbine Model

The in-house GT thermodynamic performance simulation model (Pythia-Turbomatch) was developed by Cranfield University, and has been tested with experimental data from many different types of GT engines [38,39]. The adapted component characteristic maps [40,41] of major engine components, including compressors and turbines, have been implanted into the zero-dimensional performance model to increase the performance modeling accuracy. In addition, a diagnostics platform based on gas path analysis [39,42,43] is integrated into the GT model.

2.2.2 Parallel Dual Pressure Once-through Steam Generator Model

The parallel dual pressure OTSG performance model has been enhanced to include a fouling factor to facilitate the simulation of a degradation scenario, and validated using the MU power plant measurements [44]. Gas path analysis is used for the OTSGs in order to quantify the severity of tube fouling [45].

2.2.3 Steam Turbine Model

The schematic of the ST is shown in Fig. 1, which includes two steam flows. For convenience, the ST model is divided into two parts, the HP section, and the LP section. The HP steam flow expands to the LP steam pressure at the LP admission point. Then, the HP steam is mixed with the LP steam. The mixed steam flow will expand at the LP section of the ST, and the exhaust steam will pass to the condenser. The ST performance simulation model is described and discussed in our previous works [46,47].

2.3 Gas Turbine Hot Section Creep Life Model

The HP turbine rotor blades operate under high temperature and at high rotational speed simultaneously, which makes them the most vulnerable hot section components [48]. Creep is one of the most common failure mechanisms related to the hot section of land-based GT engines [48]. Fig. 2 shows the model structure used for creep life usage estimation, which considers the HPT blade's thermo-mechanical load. The blade is divided into four sections by five locations along its span: blade root, 25% span, 50% span, 75% span, and blade tip, as shown in Fig. 2. A thermo-mechanical analysis is conducted at each section for life estimation referred to our published model [48]. Thermal analysis is applied to predict the metal temperature of the blades. Mechanical analysis evaluates the blade stress, including centrifugal stress, pressure bending moment, and momentum bending moment, as referred to in our previous paper [48].

The time to failure, t_f, is defined by Eq. (1) based on one of the most common time-temperature parameters, the Larson-Miller parameter (LMP) which is used to estimate the creep life [49]. The specific value of LMP is decided by reference to a master curve [50] when stress is known.

$$t_f = 10^{\left(\frac{1000\,LMP}{T_m} - C\right)} \quad \textbf{(1)}$$

where t_f is time to failure in hours, T_m is the blade metal temperature in Kelvin, and C is constant that varies for different materials and applications.

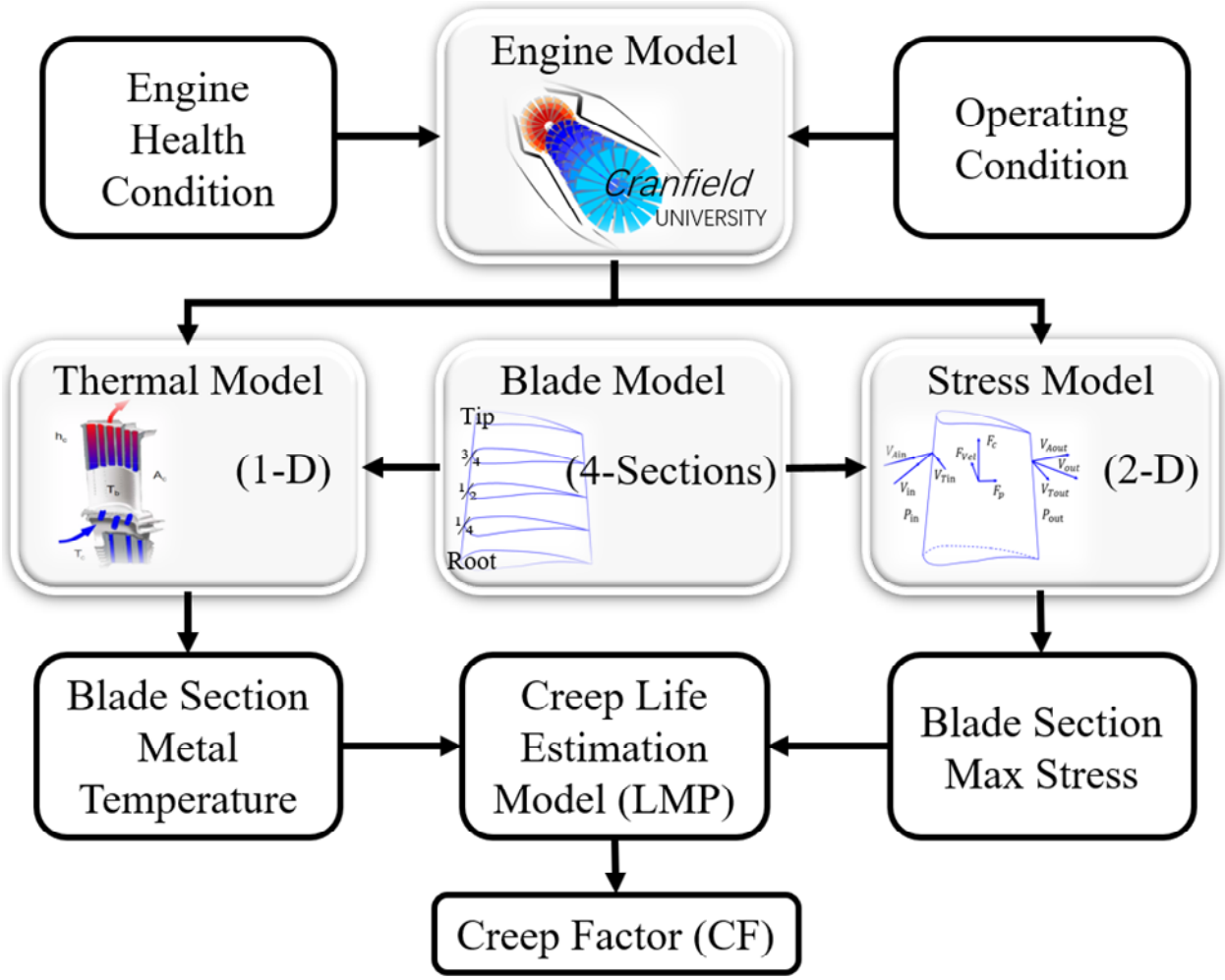

Fig. 2 Structure of the life usage estimation model.

A non-dimensional parameter, the creep factor (CF), can be obtained from Eq. **(2)** to reveal the life consumption relative to the operating condition as specified by the user [51]:

$$CF = \frac{t_f}{t_{ref}} \tag{2}$$

where t_{ref} is reference time to failure in hours at design operating conditions.

The life fraction (LF), a dimensionless parameter, is defined by Eq **(3)** [48]:

$$LF = OT/t_f \tag{3}$$

where OT denotes the operating time in hours.

A more detailed HP turbine creep life estimation algorithm is referred to our previous work [48,52].

It is worth noting that the GT engine's health condition, which will affect the thermo-mechanical load on the blades, is considered in the engine model. The degradation factor (DF) is defined by Eq. **(4)**, and is the ratio of the characteristic parameters (CP) for the actual state and ideal/clean/healthy state [53]. In this study the characteristic parameter covers component efficiency and flow capacity.

$$DF = \frac{CP_{ac}}{CP_{ideal}} \quad \textbf{(4)}$$

2.4 Emissions Model

The emissions considered in this research cover only the greenhouse gas as that is an environmental tax-related emission of industrial power plants [54]. The model uses the fuel composition method, which calculates both carbon dioxide and water vapor. The hydrocarbon stoichiometric combustion reaction is shown in Eq. **(5)** [55]. The composition of the natural gas used in this study is shown in Table 2 [56]. It should be noted that the actual composition varies slightly with respect to time and parameters characterizing the natural gas are frequently provided by the gas supplier to MU.

$$C_aH_b + (a + 0.25b) \cdot O_2 \rightarrow a \cdot CO_2 + 0.5b \cdot H_2O \quad \textbf{(5)}$$

Table 2 Natural gas composition [56]**.**

Natural Gas	Chemical Formula	Molecular Weight (g/mole)	by Mole or Volume (%)
Methane	CH_4	16.04	94.9
Ethane	C_2H_6	30.07	2.5
Propane	C_3H_8	44.10	0.2
Butane	C_4H_{10}	58.12	0.06
Pentane	C_5H_{12}	72.15	0.02
Nitrogen	N_2	28.10	1.6
Carbon Dioxide	CO_2	44.01	0.7
Oxygen	O_2	32.00	0.02
Total		324.59	100

2.5 Economic Model

This project is focused on an existing power plant and aims to optimize the operating point for the specific ambient condition, power demand, electricity price, and engine health state, so time-related economic parameters like net present value and worst annual negative cash flow are not considered here. In this study, each operating point is maintained for half an hour, which is the fiscal period for the electricity price and trading contract. The details of the economic module are as follows:

2.5.1 Maintenance and Staff Cost Model

The maintenance and staff cost model, MSC, combines maintenance cost and staff costs. It is assumed that the maintenance cost is 3.1×10^{-6} $[£/(W \cdot h)]$ [24], and the specific cost of power plant operation staff ($£/s$) which varies with operating configuration is obtained by referring to MU internal data [57].

2.5.2 Fuel Cost Model

Fuel cost (FC) is one of the major expenditures of power plant operation after the plant has been commissioned. For FC calculations, it is necessary to know the fuel flow rate (FF), fuel price (FP), and low heating value (LHV). The FC can be expressed as:

$$FC = FF \cdot FP \cdot LHV \tag{6}$$

2.5.3 Emission Cost

The emission tax (Tax_{CO_2}) is based on the state and trends of carbon pricing, which is \$28 per tonne [54]. Based on a selected constant currency rate between the US dollar and the GBP, the emission tax cost is taken as 0.0219 $£/kg$. The total carbon dioxide emission cost (EC) is calculated as:

$$EC = W_{CO_2} \cdot Tax_{CO_2} \tag{7}$$

where W_{CO_2} is the amount of carbon dioxide emission produced by a power plant (kg/s).

2.5.4 Revenue Model through Selling Electricity

The power plant obtains revenue by selling electricity to meet the island's power demand. If the generated electricity is not enough to satisfy the island's demand, excess electricity must be purchased from the UK grid via the cable. To meet the varying power demand of the island, three power supply options could be considered:

1) the island's power plant alone,
2) the cable alone, and
3) the combination of the power plant and cable.

Power supply by the cable alone is outside the scope of this study and will not be discussed further. Moreover, the power plant could also sell electricity to the UK grid. Hence, the power plant's revenue income could contain two components: the sale of electricity to the Isle of Man (island demand) and sale to the UK through the cable (cable demand). If the power generation is equal to the island's power demand, then the only income is from the island. If the power generated is more than the island's power demand, then extra income is generated by transmission through

the cable. It is necessary to mention that the export of electricity through the cable must be within the terms of the contract; otherwise additional power generated will not generate extra income [57].

$$Income = ESP \cdot PO_{CCGT} \quad \textbf{(8)}$$

where ESP is the electricity selling price and PO_{CCGT} is the power output from the CCGT power plant.

2.5.5 Spark Spread Model

The economic assessment is quantified by the spark spread (SS) trading strategy and includes four parts (income from selling electricity, maintenance and staff cost, fuel cost, and emission cost). It presents the overall economic benefit from plant operation at a specified operating time (OT), i.e., the revenue left after relevant costs are met. The higher the income and the lower the cost, the greater the spark spread. The same power output could result in a massive difference in spark spread if the electricity price is changed substantially. The SS can be calculated as:

$$SS = (Income - MSC - FC - EC) \cdot OT \quad \textbf{(9)}$$

2.6 Multi-Criteria Optimization Algorithm

A genetic algorithm (GA) is an algorithm inspired by biological evolution to search for the best solutions for constrained and unconstrained problems. In this study, the MCGA is used to find the Pareto Front, see our previous publication [58]. The initial population of chromosomes or individuals which represents the potential solutions is randomly generated. Then three major GA operators, i.e., selection, crossover, and mutation, are iteratively used in the search processes to produce better individuals and improve the quality of the whole population. Finally, a ranking method is applied based on the multiple objectives of the individuals, which is critical to select and update the Pareto Front.

Fig. 3 [59] presents the evolutionary operators and ranking method for the proposed MCGA. The selection operator is applied to obtain the next generation from the current one based on roulette wheel selection. The five sectors described in percentages in Fig. 3 (a) represent the normalization fitness of five individuals in the current generation, where the higher the fitness, the larger the area. Random generation of a number between 0 and 1 will be located at one of the five regions, and the best individuals have the greatest chance to be selected. To aid understanding of the crossover and mutation operators, binary numbers are used to demonstrate the process in Fig. 3 (b) and (c), although real numbers are used in practice. The crossover operator generates new individuals from existing ones in order to explore the available search space [59]. More specifically, Fig. 3 (b) depicts two positions (4 and 7) selected randomly

from the parents, and the genetic codes of positions 4 to 7 are swapped to generate two new individuals (children). The mutation operator, Fig. 3 (c), is adopted to ensure the presence of individuals in the search space that cannot be obtained by crossover only will be present. In practical terms, two positions are randomly selected from a parent individual and the genetic code at these two locations are swapped to obtain a new individual (child). Finally, the ranking method is employed to find the Pareto Front for the current generation. The terminal condition of the MCGA is the minimum number of the Pareto Front (400 in this study) obtained by the ranking method.

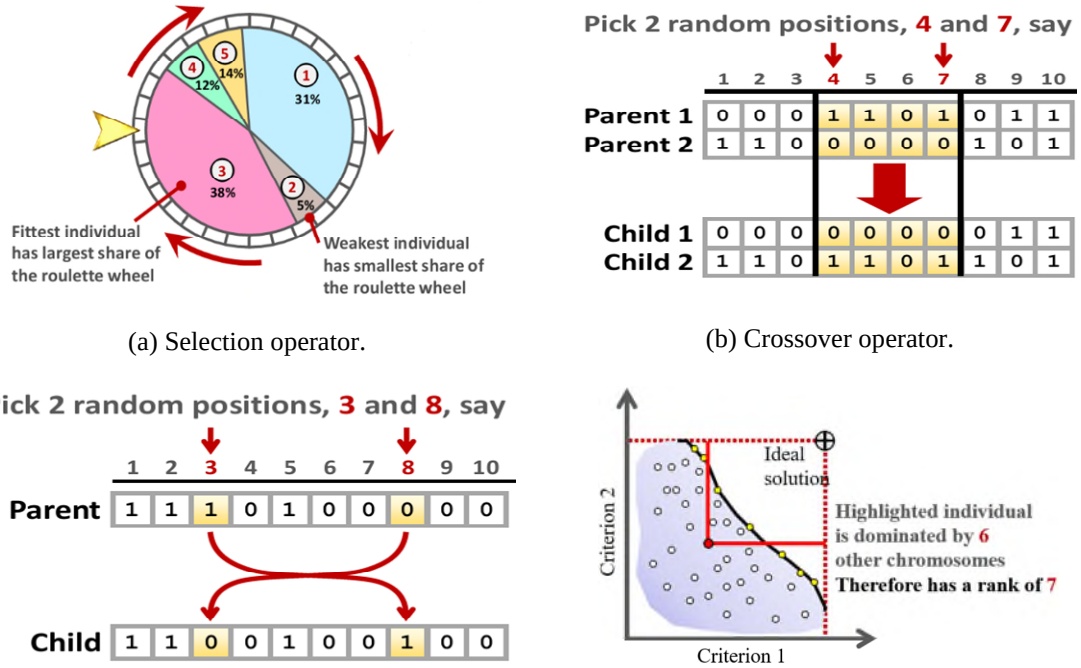

(a) Selection operator.

(b) Crossover operator.

(c) Mutation operator.

(d) Ranking method.

Fig. 3 Evolutionary operators and ranking method of MCGA [59].

2.7 Multi-Criteria Decision-Making Scheme

2.7.1 Original TOPSIS

TOPSIS is one of the most widely used multi-criteria decision-making methods, where attributes often conflict between different objectives. The detailed process is explained as follows. Firstly, the weight factor, w, [26,33–35] is defined for different criteria, as shown in Eq. **(10)**.

$$w = [w_1, \dots, w_n] \tag{10}$$

Then, the normalized weight (W) is obtained from Eq. **(11)** to give each attribute the same unit length [59].

$$W_i = \frac{w_i}{\sum_{i=1}^{n} w_i} \tag{11}$$

$\forall\, i = 1, \dots, n$, where n denotes the number of criteria of the optimization model.

The Pareto Front, y_{ij}, is normalized by Eq. **(12)**, to address the different scales for each objective.

$$z_{ij} = \frac{y_{ij}}{\sqrt{\sum_{i=1}^{n} y_{ij}^2}} \tag{12}$$

$\forall\, j = 1, \dots, m$ where m denotes the total number of Pareto Front candidates and z_{ij} is the normalized criteria value.

The weighted normalized decision matrix is obtained as:

$$a_{ij} = W_i \cdot z_{ij} \tag{13}$$

Then, the distance between a result in j-th Pareto Front and the ideal best solution (a^+), S_j^+, can be found as:

$$S_j^+ = \sqrt{\sum_{j=1}^{m} (a_{ij} - a_i^+)^2} \tag{14}$$

where a_i^+ is the ideal best solution for ith criterion.

The distance between a solution in j-th Pareto Front and the ideal worst point (a^-), S_j^-, can be obtained as:

$$S_j^- = \sqrt{\sum_{j=1}^{m} (a_{ij} - a_i^-)^2} \tag{15}$$

where a_i^- is the ideal worst solution for ith criterion.

Fig. 4 (a) illustrates the selection of optimal point from a Pareto Front based on closeness to the ideal design (CS_j) between the ideal best position (a^+) and ideal worst position (a^-) [13,60]. This is defined in Eq. **(16)**, where the larger the value, the better the solution is. The ideal best position is generally the optimal solution, with each attribute corresponding to its the best value in each solution and vice versa.

$$CS_j = \frac{S_j^-}{S_j^- + S_j^+} \tag{16}$$

As shown in Fig. 4 (a), TOPSIS is sensitive to the shape of the Pareto Front and the optimal points in orange are in the middle of the Pareto Front and close to the bottom of Pareto Front, respectively, for scenarios 1 and 2 in Fig. 4. Hence, the original TOPSIS can select an appropriate solution when the Pareto Front's shape is fixed as typically

happens when the engine health condition is fixed. For operation optimization under deteriorating power units, the Pareto Front's form is likely to be affected by the unit's health condition. It will quickly push the optimal point selected by TOPSIS to one of the endpoints of the Pareto Front.

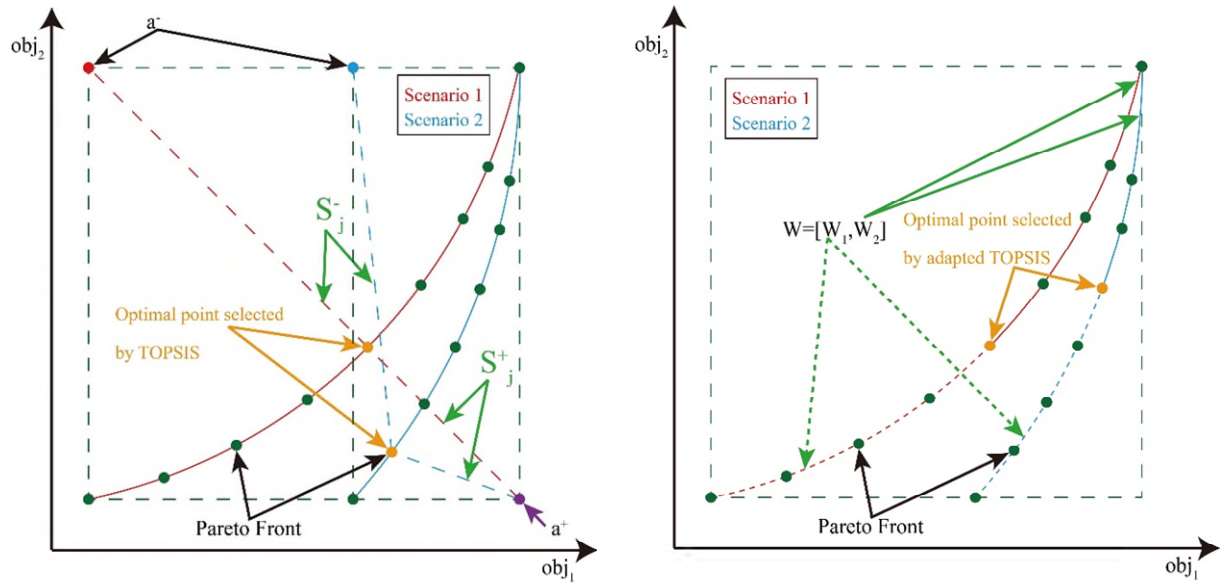

(a) Scheme of TOPSIS. (b) Scheme of adapted TOPSIS.

Fig. 4 Schematic of multi-criteria decision-making method.

2.7.2 Adapted TOPSIS

The original TOPSIS was adapted, see Fig. 4 (b), to eliminate the effect of the shape of the line forming the Pareto Front, and to target the dual decision-making criteria used in this study. The detailed process is explained as follows: The first three steps are the same as for TOPSIS and can be obtained by Eqs. **(10-12)**. Then, the z_{ij} is ranked by the selected first objective, which sorts from smallest to largest so that the other objective will automatically organize from biggest to smallest (two objectives in this study). The distance between adjacent points (d) can be obtained after ranking by Eq. **(17)**.

$$\begin{cases} d_j = 0 & j = 1 \\ d_j = \sqrt{\sum_{i=1}^{n} \left(z_{i,j-1} - z_{i,j}\right)^2} & j > 1 \end{cases} \quad \textbf{(17)}$$

The cumulative distance (cd) is calculated using Eq. **(18)**:

$$\begin{cases} cd_j = d_j & j = 1 \\ cd_j = d_j + cd_{j-1} & j > 1 \end{cases} \quad \textbf{(18)}$$

Then, the dimensionless distance (CD) is obtained from Eq. **(19)**:

$$CD_j = \frac{cd_j}{\sum_{j=1}^{m} cd_j} \quad \textbf{(19)}$$

The normalized weight will decide the arc length ratio and the closest solution. The closer the CD to the normalized weight factor, the better the operating point. Through the adapted TOPSIS, the weighted factor will act on the curved line representing the Pareto Front, rather than outside the Pareto Front so that the effect of Pareto Front line shape can be eliminated.

3. Definition of the Decision Support System

3.1 Definition of the Optimization Problem and Challenge

The challenge that the power plant operator faces is how to optimize well in advance power plant scheduling for different scenarios, considering power plant profit, GT life consumption, and emissions control.

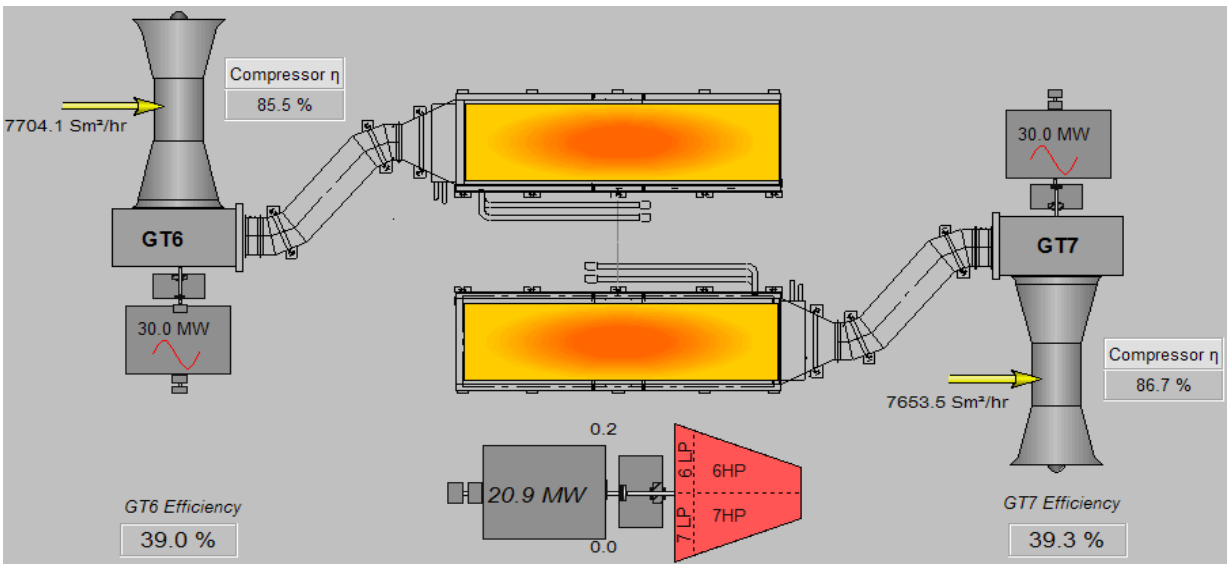

Fig. 5 Equal load operation scheme on-site at Pulrose Power Station, Manx Utilities [61]**.**

The equal load power split between the two different engine units is likely to lead to a sub-optimal solution, as it does not consider the efficiency deviation among other power machines [26]. It is clear from Fig. 5, which is a snapshot of MU's Pulrose Power Station web-based performance monitoring tool that the two parallel GT units

operate at the same power setting. However, the fuel flow rate, compressor efficiency, and engine efficiency are different [61]. No specific power load split guidelines are available for parallel GTs in the MU Pulrose Power Station, and an equal load power split is the standard practice for the engine operators. It is noted that with an equal power split scheme the hot section life consumption will be different, with the less efficient engine running under more harsh conditions. It is also worth noting that an increase of 20~25 ℃ in GT blade metal temperature will accelerate the creep life consumption by 50% approximately [62].

To assist the power plant's trading team in scheduling future plant operations and preparing improved trading contracts, predicted data based on earlier years, including profiles of ambient temperature, power demand, electricity trading prices, fuel gas prices, etc., could be used. This will optimize the plant scheduling in advance and support the trading team in obtaining the best possible operation schedules. The trading contracts will decide the total power output of the plant with 48-fiscal periods per day.

3.2 Decision Support System

The power plant operator must decide the plant's total power output as the ambient conditions, gas prices, electricity prices, and power demand for the island will fluctuate during each fiscal period in the day. Additionally, for the same total power demand, engine health could affect the CCGT power plant revenue and the GT engines' life consumption. It would be beneficial to develop a decision support platform that can suggest optimal CCGT plant operating schedules based on weighted considerations of the plant's thermo-economic and GT hot section life consumption.

3.2.1 Implementation of Decision Support for Optimization System

The architecture of the proposed decision support framework is shown in Fig. 6. The thermo-economic and lifing model is integrated with a MCGA to search the Pareto Front until the non-dominant points that form the Pareto Front reaches a specified number (400). The Pareto Front will then be transferred to the adapted TOPSIS model for decision-making based on the predefined weighting factor.

3.2.2 Optimization Variables

The CCGT power plant output is determined by the power setting for the two GTs. The bottom cycle steam turbine power will be determined automatically when the GT setting is done. The plant operator may shut down one GT together with the corresponding OTSG due to low power demand. Therefore, the variables for the CCGT power plant operation optimization are:

- GT6 power setting,
- GT7 power setting, and
- Number of GTs in operation: single GT or dual GTs with relevant steam cycle.

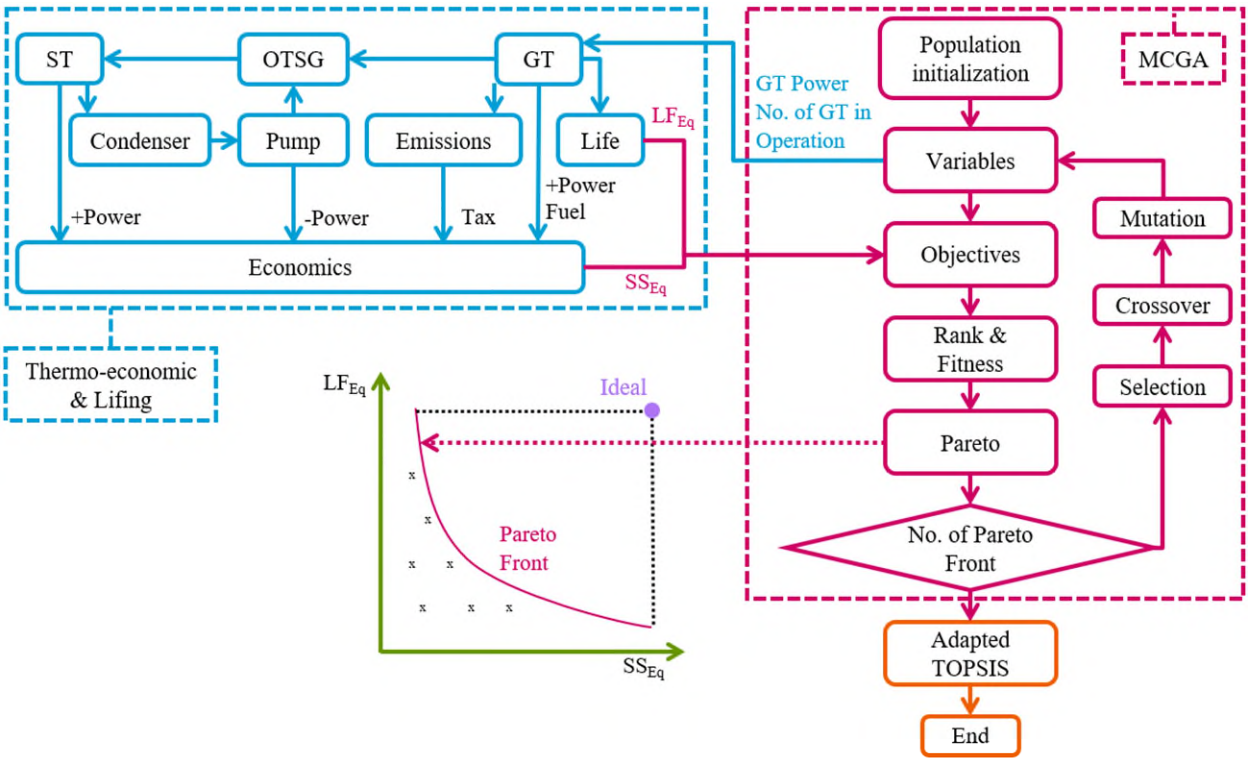

Fig. 6 Architecture of decision support system.

3.2.3 Constraints

In a real power plant, some constraints need to be satisfied to maintain a safe operation. The selected constraints here are:

- Power turbine inlet temperature: the GT hot section life usage increases exponentially with firing temperature. Hence, it is necessary to have a threshold to limit the maximum firing temperature to protect the hot section from severe creep damage. However, as there is no direct measurement of the firing temperature, the power turbine inlet temperature is used to limit the firing temperature.
- Cable transmission capacity: the installed electrical equipment limits the maximum permitted power transmission for safety reasons. Additionally, the transmission capacity is determined by demand and power supply capacity.

3.2.4 Objective Functions

The CCGT power plant's operation optimization involved two objective functions: thermo-economic performance and engine creep life consumption. The thermo-economic performance is measured by Equivalent Spark Spread, SS_{Eq}, which is defined by Eq. **(20)**.

$$SS_{Eq} = \frac{SS}{SS_{Ref}} \tag{20}$$

where SS_{Ref} is the reference spark spread used here to normalize the actual SS, due to reasons of confidentiality.

The Equivalent Creep Life Factor, LF_{Eq}, for both GT engines representing their creep life consumption is defined by Eq. **(21)**.

$$LF_{Eq} = \frac{1}{(LF_{GT6} + LF_{GT7}) \cdot LF_{Ref}} \tag{21}$$

where LF_{GT6} and LF_{GT7} represent the life fractions of GT6 and GT7 respectively, as defined by Eq. **(3)**, and LF_{Ref} is the reference value for non-dimensional representation on the grounds of MU confidentiality.

4. Application and Analysis

4.1 Case Study Description

For a typical day on the island, the electric power demand (DM_{island}) and the maximum allowed power generation (DM_{total}) are shown in Fig. 7 (a) [57]. The electricity selling price (ESP) and ambient temperature (T_{amb}) variations are shown in Fig. 7 (b) [57] as provided by MU. The typical day is divided into 48-time intervals, and each interval is 30 minutes, with each point on the figure representing the average value for a half-hour time interval between 00:00 and 24:00. When the island's power demand is less than the CCGT power plant capacity, the power plant could sell excess electricity to the UK grid via the cable. In such a situation, the DM_{total} is decided by a combination of the island's power demand and cable's power demand. If more power than DM_{total} is generated, the power plant is unlikely to receive any payment for the excess power. Three case studies with the same power demand and ambient conditions have been carried out to demonstrate the effectiveness of the proposed decision support system in Fig. 6. These are:

Case 1: To test the capacity of the proposed decision support system for GTs in a clean state when the total power demand fluctuates during the day.

Case 2: To indicate the impact of the state of health of the parallel GT engines on optimization and establish a benchmark against which comparisons will be made.

Case 3:To demonstrate the relative improvement of the hot section life consumption by optimizing operation in Case 2 as compared to operating with an equal division of power load, with the two parallel GTs in different health conditions.

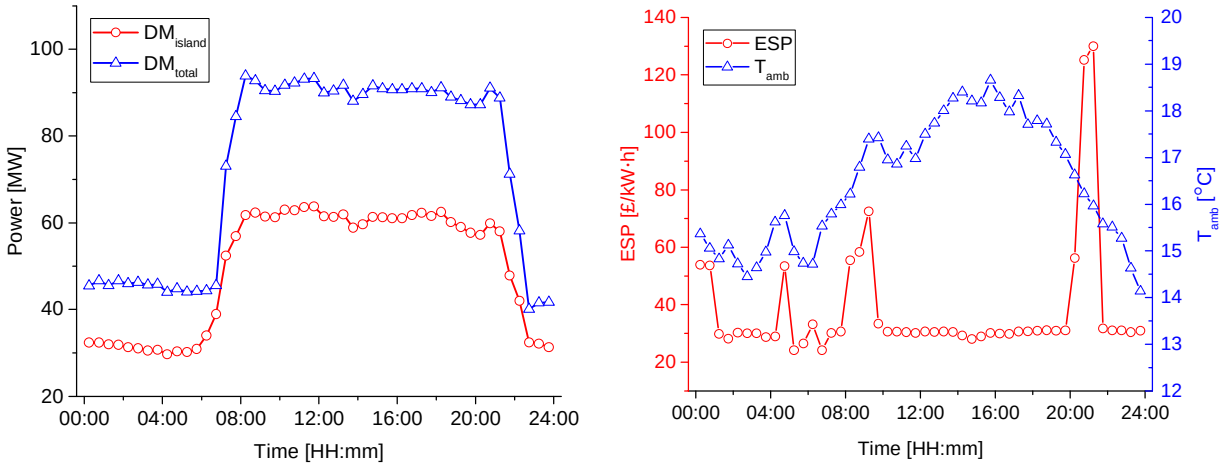

(a) Power demand during the day. (b) ESP and ambient temperature during the day.

Fig. 7 Typical Day Profile of DM_{island}, DM_{total}, ESP, and T_{amb} [57].

4.2 Case 1: Typical Day Operation Schedule Optimization Without Degradation

The operation schedule optimization is carried out for each time interval using the decision support framework to obtain the operating schedule for the whole day when both GTs are in a healthy state. Two typical scenarios are discussed, and an optimal operation schedule for the whole day is demonstrated.

4.2.1 Low power Demand - Early Morning and Late Evening

The low power demand scenario typically occurs between 0:00 hour and 7:00 hours (Fig. 7 (a)). An example is during the interval between 00:00 and 00:30 hour when the island's power demand and cable demand are 32.37 and 13.08 MW, respectively, and the maximum allowed power generation (total demand) DM_{total} is 45.45 MW (Table 3). It is not difficult for the plant operator to decide that one GT should be operated and have the steam turbine generate the necessary power. However, it is challenging for the power plant operator to determine what level of electric power up to 45.45 MW should be generated in order to achieve the best technical, economic, and lifing benefits. This is because the economic benefits and the engine life consumption will differ in three scenarios:

1) When the power generated is less than the island power demand so that the shortfall of the electricity will be imported via the cable,
2) The power generated is equal to the island demand without electricity transmission along the cable,
3) When the power generated is more than the island's power demand so the excess electricity will be sold to the UK national grid through the cable.

Table 3 Operation Condition between 00:00 and 00:30.

Parameter	Value	Unit
Island Demand	32.37	MW
Cable Demand	13.08	MW
Total Demand	45.45	MW
ESP	53.95	$£/(kW \cdot h)$

Fig. 8 shows the derived Pareto Front and GT power setting as the results of the operation optimization when the optimization objectives are the equivalent spark spread (SS_{Eq}) and the engine equivalent life factor (LF_{Eq}). The optimization results indicate that only one GT should be in operation. It is clear from Fig. 8 that only GT6 (*full-time engine* set) is recommended to produce a power output between 23 MW and 32 MW along the whole Pareto Front (PO_{GT6}), while GT7 (*peak load engine* set) supplies zero power. Finally, the adapted TOPSIS method is used to determine the final operating point by the specified weight factor between SS_{Eq} and LF_{Eq} this is shown in Fig. 8 by the star.

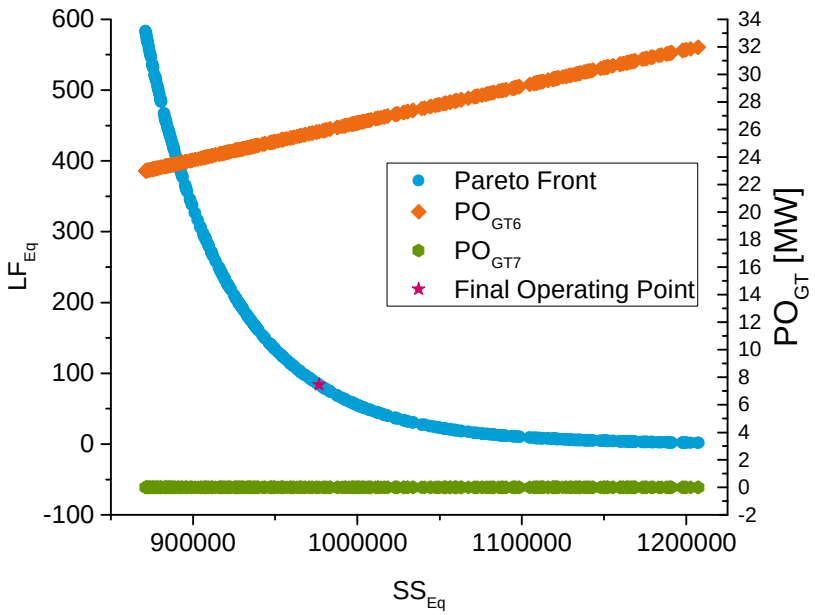

Fig. 8 Operation optimization and decision-making for low power demand without degradation.

4.2.2 High Power Demand – Middle of the Day

The second example considers the operating interval between 11:30 and 12:00, when the rated CCGT power output lies within the island demand and total demand, as shown in Table 4. During this period, the power plant could generate more than enough power to satisfy the island demand and sell extra electricity to the UK grid, or it could only generate electricity to meet part of the demand and import the rest via the cable, and/or generate the power equal to the island demand and not require any power transmitted through the cable. There is a wide range of options for the plant operator to choose from, depending on the plant operation economics, ambient conditions, engine health, and operating constraints such as limitation of GT firing temperature.

Table 4 Operation condition between 11:30 and 12:00.

Parameter	Value	Unit
Island Demand	63.75	MW
Cable Demand	29.55	MW
Total Demand	93.30	MW
ESP	30.15	£/(kW.h)

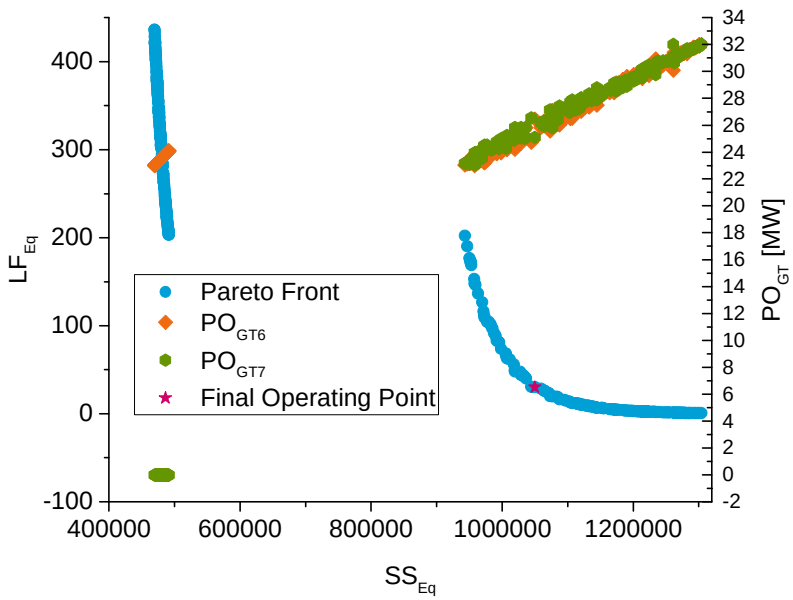

Fig. 9 Operation optimization and decision-making for high power demand without degradation.

By searching the optimal solutions of the power plant operation against the two objective functions, the Pareto Front obtained by the decision support system is as shown in Fig. 9. All potentially optimal operating points appear on two discontinuous lines. The line on the left side refers to when the plant operates only a single GT driving the

steam cycle with low power output. Such operation results in a low engine life consumption as indicated by high LF_{Eq} but has poor economic benefits indicated by the low value of SS_{Eq}. On the other hand, the line on the right-hand side of the graph refers to the situation where two GTs operate together with the steam turbine resulting in high economic benefits as indicated by high values of SS_{Eq} at the Pareto Front, but relatively high life consumption as shown by the low values of LF_{Eq}. It is also shown in Fig. 9 that the power setting of the two GT outputs should be close to each other to minimize life consumption for the two engines without compromising the SS_{Eq}. By applying the adapted TOPSIS, the final operating point is obtained and shown by a star on Fig. 9, which is a compromise between economic benefit and life consumption according to the specified weight factor.

4.2.3 Typical Day Operation Schedule

Sections 4.2.1 and 4.2.2 have presented the results and analysis of two typical operation scenarios obtained from the decision support framework, and in each case, the best operation point is suggested. Such a process has also been applied to all-time intervals of the typical day, and the corresponding optimal power plant operation schedule is shown in Fig. 10. It was found that there were two-time intervals (06:30-07:00, and 22:00-22:30) during which the power plant should import electricity from the grid to help satisfy the island's demand. The reason for this lies in the fact that the PO_{CCGT} will exceed the DM_{total} when operating two GTs but less than the DM_{island} when operating one GT. Hence, the power plant should operate a single GT and import electricity from the grid.

Fig. 11 shows SS_{Eq} and LF_{Eq} for all the operation points in the obtained operating schedule. It is worth noting that this operation scheme is a compromise between economic benefits and life consumption based on the same weighted factor for the whole day. It shows that in the early morning and late evening the power plant would operate only one GT and corresponding steam cycle, and therefore, generally, the SS_{Eq} would be low and the LF_{Eq} would be high, while during mid-day, the power plant would operate with two turbines driving the steam cycle and the SS_{Eq} would be high and LF_{Eq} would be low. However, there are two exceptions.

The first at times earlier than 07:00 (before the $15th$ point on the plot), where the power plant could operate only a single GT with the corresponding steam cycle at a relatively high-power setting. At 07:00-07:30 (the $15th$ point) the second GT could be switched on to share the increased power demand and operate at a relatively low power setting. Subsequently, the power demand rises further and requires the GTs to run at relatively high-power.

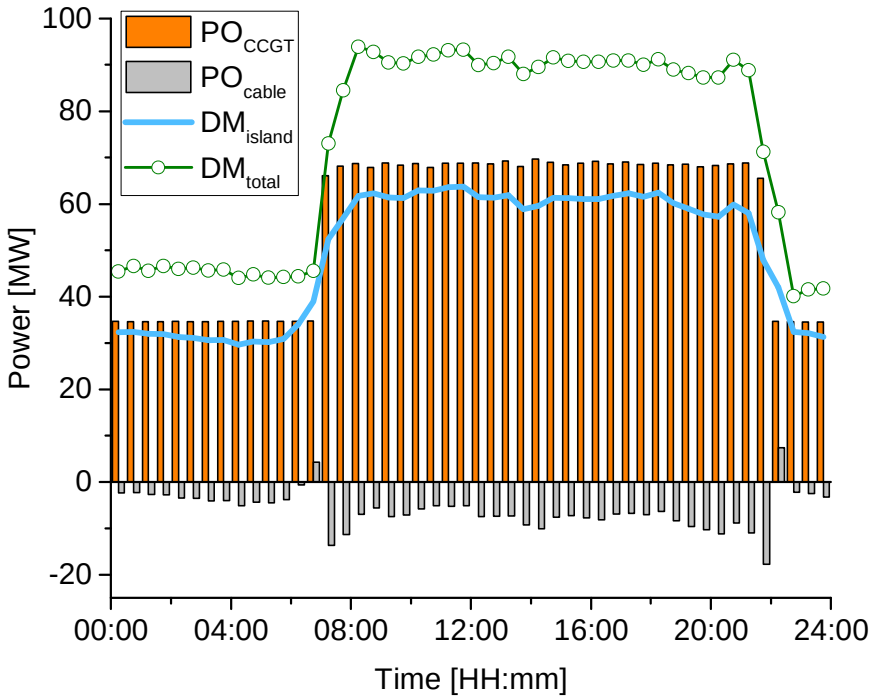

Fig. 10 Optimal trading schedule without plant degradation.

The second is at 21:30-22:00 (the 44th point) when there is a reduction in power demand, but the power plant is still able to operate with both GTs together with the steam cycle though at relatively low power settings. After this point, the power plant would shut down one of the engines due to further reduction in power demand.

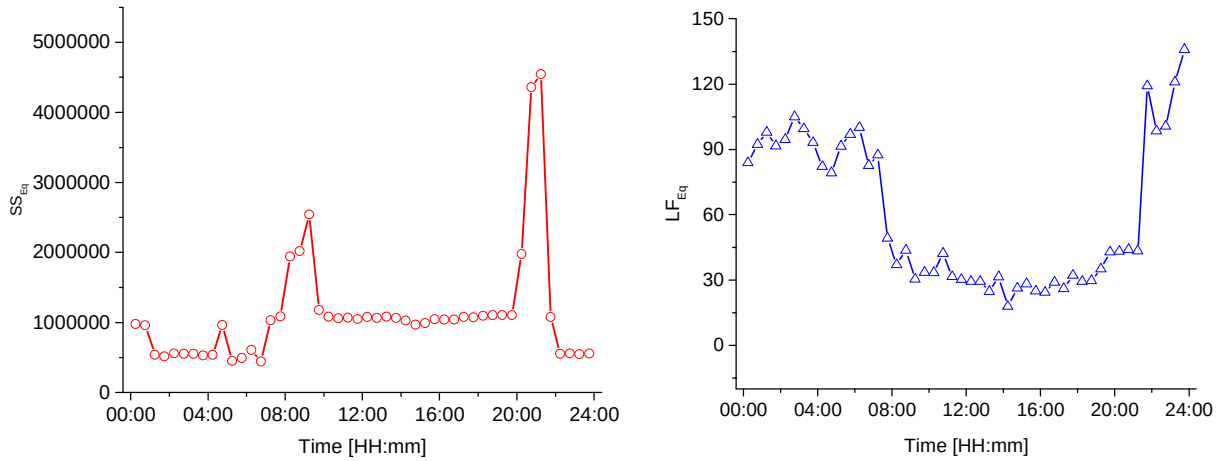

(a) SS_{Eq} during the day. (b) LF_{Eq} during the day.

Fig. 11 Optimized SS_{Eq} and LF_{Eq} without plant degradation.

4.3 Case 2: Typical Day Operation Schedule Optimization Under Degradation

Even though two identical GTs were installed in the same power plant, their health states may deteriorate at different rates, for example if only GT6 (*full-time engine* set) is operated to satisfy the low power demand in the early

morning and late evening, and GT7 (*peak load engine* set) joins on-duty in the middle of the day. Then the two GTs would consume their creep life at different rates for the same power setting due to different cumulative running times and operation strategies. Fig. 12 (a) shows how the creep factor of the GTs may be affected by the GT compressor degradation at power settings of 32 MW and 26 MW. When the GT compressor (efficiency and flow capacity indices) deteriorates from 0% to 5%, the consumption rate of GT creep life will increase exponentially. Moreover, the effect of compressor degradation on hot section creep life is more severe at the low power setting, as the relative change of gas temperature is larger at low power settings where the efficiency of components is poor.

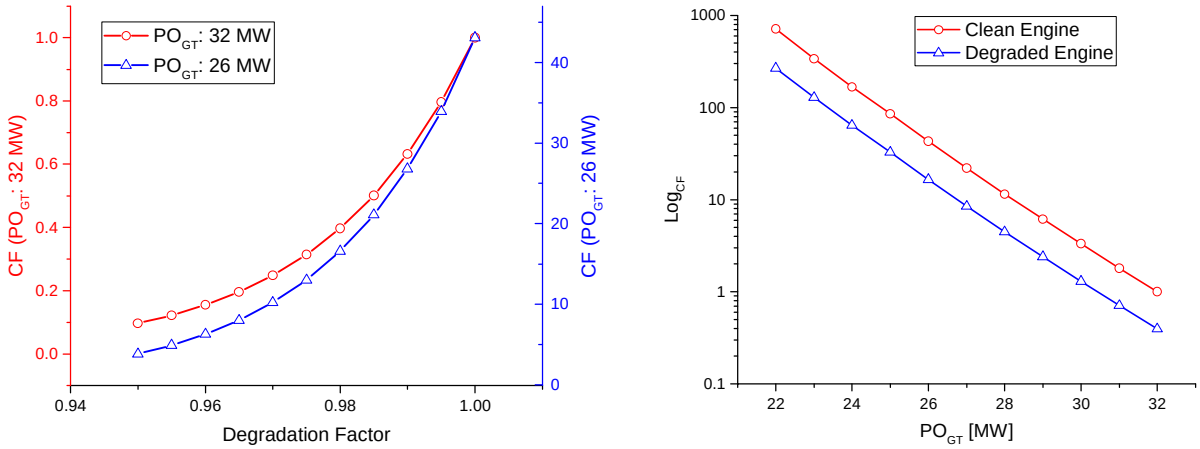

(a) Effect of degradation on CF. (b) Effect of power setting on CF.

Fig. 12 Effect of GT degradation factor and power setting on creep factor.

Fig. 12 (b) shows how the logarithmic CF of the GT changes with respect to power output for both the healthy engine and an engine with compressor degradation of 2%. It shows that a lower power setting of the degraded engine can have the same CF as that of a high-power setting of a healthy engine. In other words, lowering the power setting for a degraded engine can extend the engine creep life and compensate for the faster life consumption caused by engine degradation. Thus, it is beneficial to guide power plant operation to balance the creep life consumption between the two engines when the two GTs have different health conditions. The following case demonstrates the CCGT power plant's operation optimization if one of the GT is degraded.

Table 5 Assumed GT6 engine degradation.

Component	Degradation Type	Parameter	Degradation Level [%]
HPC	Fouling	Efficiency Index	-2.0
		Flow capacity Index	-2.0
HPT	Fouling	Efficiency Index	-0.5
		Flow capacity Index	-1.5

To represent the different engine health states caused by different running times and operating schemes, it is assumed that GT6 has both compressor and HP turbine degradation, as shown in Table 5, while GT7 is in a clean/nominal condition. The optimal operation of the CCGT power plant is searched for, again using the proposed decision support system with the optimization of both LF_{Eq} and SS_{Eq}. Fig. 13 shows the obtained Pareto Front, PO_{GT6}, and PO_{GT7} on the LF_{Eq}- SS_{Eq} graph. It is evident that the clean engine GT7 tends to operate at a higher power setting when compared with the degraded engine GT6, to give a better power split between the two engine units when including consideration of life consumption. Fig. 13 shows the final operating power of each of the GTs as determined by the adapted TOPSIS. The result is a compromise between life factor and spark spread based on the predefined weighting factors.

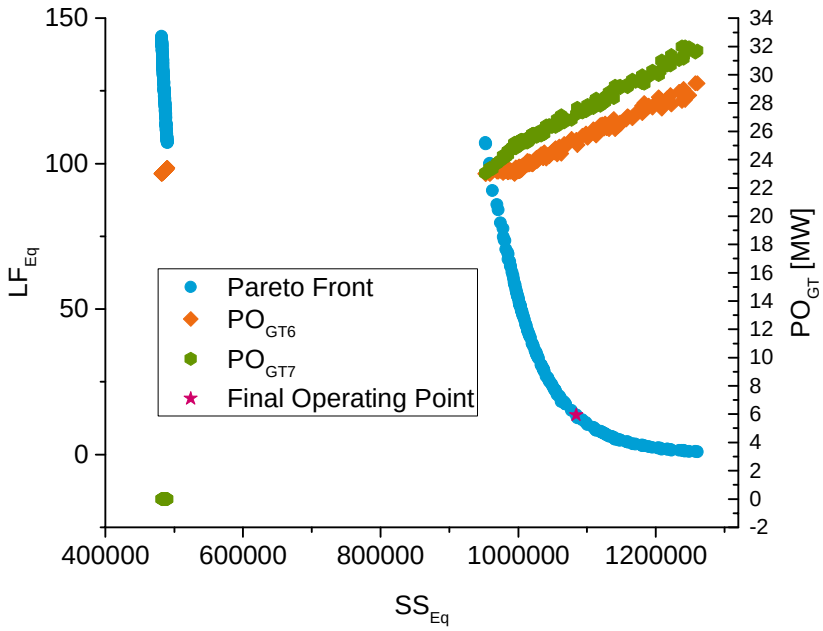

Fig. 13 Operation optimization and decision-making with Degradation.

The same optimization has been applied to a typical day's operation, shown in Fig. 7, to seek an optimal operation schedule. The results are shown in Fig. 14, where the decision support system suggested the trading schedule. For each of the 48-time slots, the final operating point is decided by the adapted TOPSIS and Pareto Front obtained by MCGA.

To demonstrate the benefits of the MCGA, a comparison of the optimal operation schedules between the clean and the degraded power plant was carried out. The SS_{Eq} and LF_{Eq} are showed in Fig. 15 (a) and Fig. 15 (b) for both clean (Case 1) and degraded (Case 2) conditions, respectively. It is worth mentioning that the predefined weighted factor is

the same as the clean state in Case 1 between SS_{Eq} and LF_{Eq}. It was found that the SS_{Eq} values were very close for both the clean and degraded conditions, see Fig. 15 (a), illustrating the advice of the proposed decision-support system. For LF_{Eq}, the life consumption is much greater under the degraded condition compared with the clean state in the early morning and late at night. This is because only one GT engine with a deteriorated state, i.e., GT6 and the corresponding steam cycle, is running. For the points where both GTs are operating together with the steam cycle, the LF_{Eq} at degraded condition is relatively close to the clean state, which demonstrates the benefit of the decision support framework.

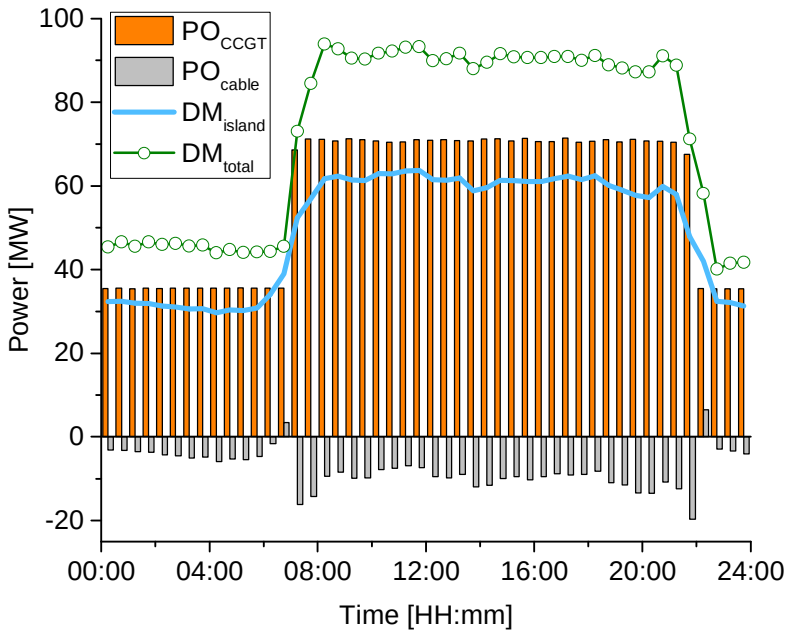

Fig. 14 Suggested trading schedule under degradation.

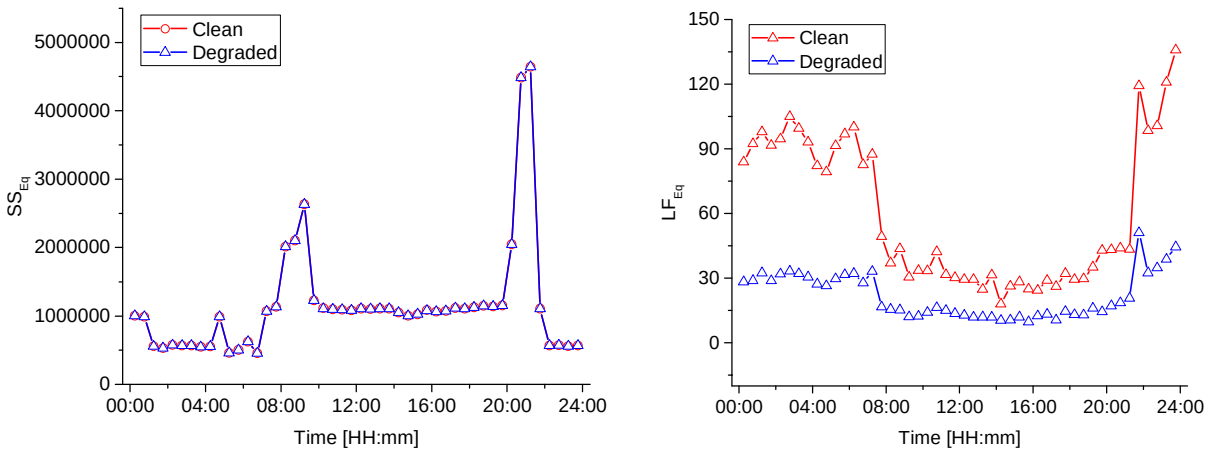

(a) SS_{Eq} during the day. (b) LF_{Eq} during the day.

Fig. 15 Optimized SS_{Eq} and LF_{Eq} with degradation.

4.4 Case 3: Improvement of Engine Life by Decision Support System

In order to demonstrate the advantages of the proposed decision-making system further, a comparison between optimized operation results and an equal load power split operation scheme was conducted. The total power demand in the early morning and late evening are relatively low, and only one GT will suffice so here only high power demand is considered in each fiscal period with two GTs running simultaneously. As the decision-supporting system is based on a two-criteria optimization scheme, it is necessary to keep one constant, and the problem becomes a typical one dimension problem. In this case, the equal load power split operation is applied to maintain the same level of SS_{Eq} with Case 2, as obtained in Fig. 15 (a). In other words, the two GTs keep the same power setting as when GT6 was in the degraded condition (Table 5) and GT7 was in a clean/healthy state to obtain the same SS_{Eq} from the optimal operation schedule as in Case 2. Then, the LF_{Eq} under an equal load power split operation could improve which demonstrates one of the advantages of the optimized operation scheme.

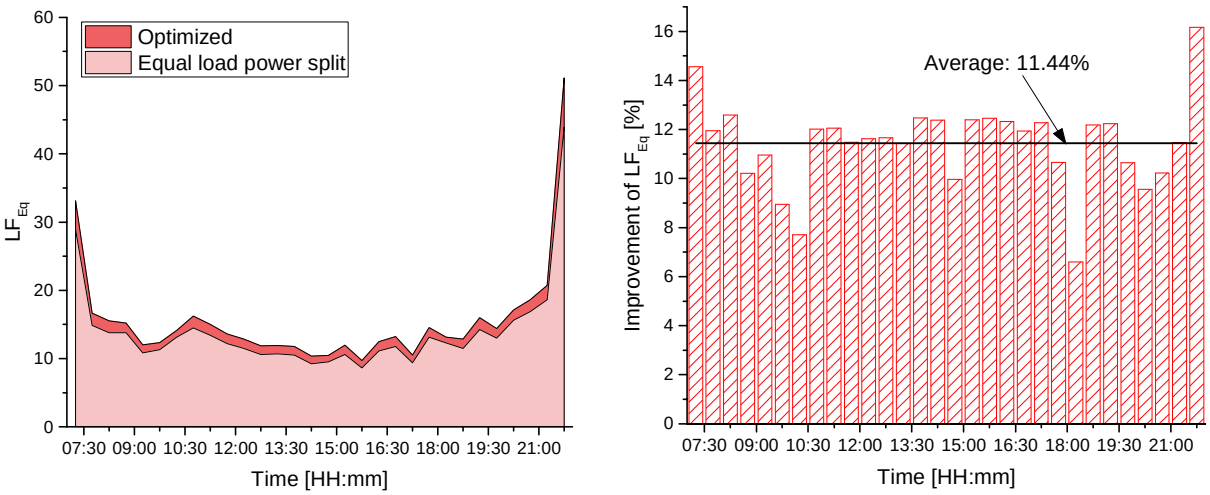

(a) Comparison of LF_{Eq}. (b) Improvement of LF_{Eq} by optimization.

Fig. 16 Comparison between optimized and equal load power split operations.

The benefits of considering life consumption on the optimal operation schedule are shown in Fig. 16 (a) where the LF_{Eq} corresponding to the optimal operation schedule is increased, in comparison with that of the equal load power split operation schedule. Fig. 16 (b) shows the improvement of LF_{Eq} in percentage terms compared to those of the equal load power split operation schedule. The average improvement over all time slots is 11.44% when both GTs are in operation during the high-power demand period for the typical day. It is evident that the operation optimization system could help to achieve the same economic benefit without over-consuming the GT hot section life.

In practice, several actions need to be considered to implement the proposed decision support system successfully. Ensuring appropriate system modeling, and fault diagnosis for primary units in the plant should be a priority for operation optimization. The fault level of primary units needs to be updated regularly, especially when maintenance actions are carried out. Moreover, great effort is required to ensure an accurate prediction of the island's power demand, maximum allowed power generation, electricity trading prices, and fuel gas prices to ensure operation optimization by the plant trading team in advance.

5. Conclusions

This study develops a techno-economic methodology for the optimization of power plant operation considering life usage and economic benefits. The framework was applied to the CCGT power plant at Manx Utilities in the UK, and the operation schedule optimization has been demonstrated for a typical day's operation with the total power demand split between two gas turbines considering gas turbine degradation, hot section life consumption, ambient conditions, and electricity price. The thermo-economic and lifing models were developed to establish a decision support system that aims to optimize the spark spread and lifing factor.

The power plant's techno-economic performance was investigated by searching the Pareto Front through a multi-criteria genetic algorithm. Based on the set of efficient solutions, the selection process was conducted by the adapted TOPSIS method. The results of the case studies demonstrate and illustrate the following:

1) The developed decision support system offers a guide for the plant trading team for signing trading contracts well in advance to get the best possible operation scheme.
2) The TOPSIS method has been adapted for multi-criteria decision-making to eliminate the effects of Pareto Front shape under different scenarios.
3) The results suggest running the healthier engine of the two GT engines at a relatively higher power output to balance the engines' life consumption without compromising the power demand and economic benefits.
4) A comparison between operation schedules with equal power split and optimized uneven power split of the two engines shows that an average improvement of 11.44% in equivalent life factor can be achieved without losing the spark spread benefits for the given test condition and assumed engine degradation.

In summary, a decision support framework has been established for thermo-economic and life consumption optimization of a CCGT power plant for daily power plant operation which offers the potential to change control of

the process from experience-based to model-based. Such a schedule optimization method can be applied to different types of CCGT power plants to achieve improved economic benefits and extend operating life to reduce maintenance costs.

Acknowledgments

The authors would like to acknowledge the support and advice, and the data provided by Manx Utilities, Isle of Man, the United Kingdom. The authors would also like to acknowledge the constructive comments, and suggestions provided by the anonymous reviewers that greatly improved the quality of the article.

References

[1] U.S. Energy Information Administration. International Energy Outlook 2019 with projections to 2050 International. 2019.

[2] International Energy Agency. Electricity Information: Overview. 2018.

[3] Zhang Y, Huang Z, Zheng F, Zhou R, Le J, An X. Cooperative optimization scheduling of the electricity-gas coupled system considering wind power uncertainty via a decomposition-coordination framework. Energy 2020;194.

[4] Tahan M, Tsoutsanis E, Muhammad M, Abdul Karim ZA. Performance-based health monitoring, diagnostics and prognostics for condition-based maintenance of gas turbines: A review. Appl Energy 2017;198:122–44.

[5] Al-Zareer M, Dincer I, Rosen MA. Analysis and assessment of the integrated generation IV gas-cooled fast nuclear reactor and copper-chlorine cycle for hydrogen and electricity production. Energy Convers Manag 2020;205.

[6] Jalili M, Chitsaz A, Hashemian M, Rosen MA. Economic and environmental assessment using emergy of a geothermal power plant. Energy Convers Manag 2021;228.

[7] Aminyavari M, Mamaghani AH, Shirazi A, Najafi B, Rinaldi F. Exergetic, economic, and environmental evaluations and multi-objective optimization of an internal-reforming SOFC-gas turbine cycle coupled with a Rankine cycle. Appl Therm Eng 2016;108:833–46.

[8] Baccioli A, Antonelli M, Desideri U. Technical and economic analysis of organic flash regenerative cycles (OFRCs) for low temperature waste heat recovery. Appl Energy 2017;199:69–87.

[9] Brighenti GD, Orts-gonzalez PL, Sanchez-de-leon L, Zachos PK. Design Point Performance and Optimization of Humid Air Turbine Power Plants. Appl Sci 2017;7:413.

[10] Ondeck A, Edgar TF, Baldea M. A multi-scale framework for simultaneous optimization of the design and operating strategy of residential CHP systems. Appl Energy 2017;205:1495–511.

[11] Palagi L, Sciubba E, Tocci L. A neural network approach to the combined multi-objective optimization of the thermodynamic cycle and the radial inflow turbine for Organic Rankine cycle applications. Appl Energy 2019;237:210–26.

[12] Frate GF, Ferrari L, Lensi R, Desideri U. Steam expander as a throttling valve replacement in industrial plants: A techno-economic feasibility analysis. Appl Energy 2019;238:11–21.

[13] Yang Y, Huang Y, Jiang P, Zhu Y. Multi-objective optimization of combined cooling, heating, and power systems with supercritical CO2 recompression Brayton cycle. Appl Energy 2020;271.

[14] Mohammadi K, Ellingwood K, Powell K. A novel triple power cycle featuring a gas turbine cycle with supercritical carbon dioxide and organic Rankine cycles: Thermoeconomic analysis and optimization. Energy Convers Manag 2020;220:113123.

[15] Liu Z, He T. Exergoeconomic analysis and optimization of a Gas Turbine-Modular Helium Reactor with new organic Rankine cycle for efficient design and operation. Energy Convers Manag 2020;204:112311.

[16] Su R, Yu Z, Xia L, Sun J. Performance analysis and multi-objective optimization of an integrated gas turbine/supercritical CO2 recompression/transcritial CO2 cogeneration system using liquefied natural gas cold energy. Energy Convers Manag 2020;220:113136.

[17] Chen L, Shen J, Ge Y, Wu Z, Wang W, Zhu F, et al. Power and efficiency optimization of open Maisotsenko-Brayton cycle and performance comparison with traditional open regenerated Brayton cycle. Energy Convers Manag 2020;217.

[18] Movahed P, Avami A. Techno-economic optimization of biogas-fueled micro gas turbine cogeneration systems in sewage treatment plant. Energy Convers Manag 2020;218.

[19] Pan P, Yuan C, Sun Y, Yan X, Lu M, Bucknall R. Thermo-economic analysis and multi-objective optimization of S-CO2 Brayton cycle waste heat recovery system for an ocean-going 9000 TEU container ship. Energy Convers Manag 2020;221:113077.

[20] Zare V. Performance improvement of biomass-fueled closed cycle gas turbine via compressor inlet cooling using absorption refrigeration; thermoeconomic analysis and multi-objective optimization. Energy Convers Manag 2020;215.

[21] Song Z, Liu T, Lin Q. Multi-objective optimization of a solar hybrid CCHP system based on different operation modes. Energy 2020;206.

[22] Badshah N, Al-attab KA, Zainal ZA. Design optimization and experimental analysis of externally fired gas turbine system fuelled by biomass. Energy 2020;198.

[23] Seme S, Sredenšek K, Praunseis Z, Štumberger B, Hadžiselimović M. Optimal price of electricity of solar power plants and small hydro power plants – Technical and economical part of investments. Energy 2018;157:87–95.

[24] Walsh PP, Fletcher P. Gas turbine Performance. Second Edi. Oxford: Blackwell Science; 2004.

[25] Wang A, Liu J, Zhang S, Liu M, Yan J. Steam generation system operation optimization in parabolic trough concentrating solar power plants under cloudy conditions. Appl Energy 2020;265.

[26] Milosavljevic P, Marchetti AG, Cortinovis A, Faulwasser T, Mercangöz M, Bonvin D. Real-time optimization of load sharing for gas compressors in the presence of uncertainty. Appl Energy 2020;272:114883.

[27] Faridpak B, Farrokhifar M, Murzakhanov I, Safari A. A series multi-step approach for operation Co-optimization of integrated power and natural gas systems. Energy 2020;204.

[28] Zhou S, Zhuang W, Wu Z, Gu W, Zhan X, Liu Z, et al. Optimized scheduling of multi-region Gas and Power Complementary system considering tiered gas tariff. Energy 2020;193.

[29] Chen X, Wang C, Wu Q, Dong X, Yang M, He S, et al. Optimal operation of integrated energy system considering dynamic heat-gas characteristics and uncertain wind power. Energy 2020;198:117270.

[30] Majdi Yazdi MR, Ommi F, Ehyaei MA, Rosen MA. Comparison of gas turbine inlet air cooling systems for several climates in Iran using energy, exergy, economic, and environmental (4E) analyses. Energy Convers Manag 2020;216.

[31] Kim MJ, Kim TS, Flores RJ, Brouwer J. Neural-network-based optimization for economic dispatch of combined heat and power systems. Appl Energy 2020;265:114785.

[32] Rezazadeh Reyhani M, Alizadeh M, Fathi A, Khaledi H. Turbine blade temperature calculation and life estimation - a sensitivity analysis. Propuls Power Res 2013;2:148–61.

[33] Thanganadar D, Asfand F, Patchigolla K. Thermal performance and economic analysis of supercritical Carbon Dioxide cycles in combined cycle power plant. Appl Energy 2019;255:113836.

[34] Gomes EEB, Pilidis P, Polizakis a. L. Generation Schedule Optimisation for Gas Turbine Power Systems. Vol. 2 Turbo Expo 2007, Montreal, Canada: ASME Turbo Expo; 2007, p. 989–98.

[35] Han Z, Zhang H, Wu D, Ma F. Performance optimization for a novel combined cooling, heating and power-organic Rankine cycle system with improved following electric load strategy based on different objectives. Energy Convers Manag 2020.

[36] Manx Utilities. Welcome to Pulrose Power Station. Pulrose Power Stn 2020. https://www.manxutilities.im/media/1138/welcome-to-pulrose-power-station.pdf (accessed August 3, 2020).

[37] Innovative Steam Technologies. IST-2015-Manx-Electricity-Authority 2005. https://otsg.com/ist-uploads/2015/04/2015-Manx-Electricity-Authority.pdf (accessed October 19, 2020).

[38] Rubie JS, Li YG, Jackson AJB. PERFORMANCE SIMULATION AND ANALYSIS OF A GAS TURBINE ENGINE USING DROP-IN BIO-FUELS. ASME Turbo Expo Turbomach. Tech. Conf. Expo., Oslo, Norway: 2018, p. 1–12.

[39] Tsoutsanis E, Li YG, Pilidis P, Newby M. Non-linear model calibration for off-design performance prediction of gas turbines with experimental data. Aeronaut. J., vol. 121, 2017, p. 1758–77.

[40] Li YG, Ghafir MFA, Wang L, Singh R, Huang K, Feng X, et al. Improved multiple point nonlinear genetic algorithm based performance adaptation using least square method. J Eng Gas Turbines Power 2012;134.

[41] Tsoutsanis E, Meskin N, Benammar M, Khorasani K. A component map tuning method for performance prediction and diagnostics of gas turbine compressors. Appl Energy 2014;135:572–85.

[42] Li YG, Korakianitis T. Nonlinear weighted-least-squares estimation approach for gas-turbine diagnostic applications. J Propuls Power 2011;27:337–45.

[43] Tsoutsanis E, Hamadache M, Dixon R. Real-Time Diagnostic Method of Gas Turbines Operating Under Transient Conditions in Hybrid Power Plants. J Eng Gas Turbines Power 2020;142:1–10.

[44] Chen YZ, Li YG, Newby MA. Performance simulation of a parallel dual-pressure once-through steam generator. Energy 2019;173:16–27.

[45] Chen YZ, Li YG, Newby MA. Gas path diagnostics for a once-through steam generator. Proc. ASME Turbo Expo, vol. 3, Phoenix, Arizona, USA: 2019, p. 1–11.

[46] Wang Z, Li YG, Li S. Performance simulation of 3-stage gas turbine CHP plant for marine applications. Proc ASME Turbo Expo 2016;3:1–11.

[47] Wang Z, Lei H, Li YG, Li S, Wang W. Optimization analysis of combined heat and power plant of multistage gas turbine for marine applications. Proc ASME Turbo Expo 2018;3.

[48] Saturday EG, Li YG, Ogiriki EA, Newby MA. Creep-life usage analysis and tracking for industrial gas turbines. J Propuls Power 2017;33:1305–14.

[49] Larson FR, Miller J. A time-temperature relationship for rupture and creep stresses, Transactions of ASME; 1952, p. 765–75.

[50] Wood JH, Shores DA, Minneapolis NRL. CAST NICKEL-BASE ALLOY. US 6,416,596 B1, 2002.

[51] Abdul Ghafir MF, Li YG, Singh R, Huang K, Feng X. Impact of Operating and Health Conditions on Aero Gas Turbine: Hot Section Creep Life Using a Creep Factor Approach. Vol 3 Control Diagnostics Instrumentation; Cycle Innov Mar 2010:533–45.

[52] Ogiriki EA, Li YG, Nikolaidis T. Prediction and Analysis of Impact of Thermal Barrier Coating Oxidation on Gas Turbine Creep Life. J Eng Gas Turbines Power 2016;138:1–9.

[53] Chen YZ, Zhao XD, Xiang HC, Tsoutsanis E. A sequential model-based approach for gas turbine performance diagnostics. Energy 2021;220:119657.

[54] WorldBank, Ecofys. State and Trends of Carbon Pricing. vol. 88284. Washington DC: World Bank; 2015.

[55] Goodger EM. An Overview of Heat Engines and Their Fuels. Landfall Press; 2014.

[56] Demirbas A. Methane Gas Hydrate. Springer; 2010.

[57] Newby M, Stigant G. CCGT Operation Report (Internal report; no support for external access). Isle of Man: Manx Utilities; 2018.

[58] Li YG. Diagnostics of power setting sensor fault of gas turbine engines using genetic algorithm. Aeronaut J 2017;121:1109–30.

[59] Dalton J. Optimisation Lectures. Engineering Design Centre, University of Newcastle upon Tyne: 2014.

[60] Zhang S, Lin Z, Ai Z, Huan C, Cheng Y, Wang F. Multi-criteria performance optimization for operation of stratum ventilation under heating mode. Appl Energy 2019;239:969–80.

[61] Pulrose Power Station (Internal network; no support for external access). MEA Web Health Monitoring Interface. Manx Util Isel Man 2016. http://pulweb/webhmi/main.htm (accessed January 14, 2016).

[62] Nagarajaiah V, Banerjee N, Ajay Kumar BS, Gowda KK. Effect of blade deflection angles, pressure drop, flow and work co-efficients on stage performance of a gas turbine shrouded HP compressor blade. Am Soc Mech Eng Power Div POWER 2016;2016-Janua:1–11.

Techno-economic evaluation and optimization of CCGT power plant: a multi-criteria decision support system

Chen, Yu-Zhi

2021-04-19

Chen Y-Z, Li Y-G, Tsoutsanis E, et al., (2021) Techno-economic evaluation and optimization of CCGT power plant: a multi-criteria decision support system. Energy Conversion and Management, Volume 237, June 2021, Article number 114107

https://doi.org/10.1016/j.enconman.2021.114107